Author/s:
Horsnell, HL;Cao, WHJ;Belz, GT;Mueller, SN;Alexandre, YO

Title:
The transcription factor SpiB regulates the fibroblastic reticular cell network and CD8+ T-cell responses in lymph nodes

Date:
2024-04-01

Citation:
Horsnell, H. L., Cao, W. H. J., Belz, G. T., Mueller, S. N. & Alexandre, Y. O. (2024). The transcription factor SpiB regulates the fibroblastic reticular cell network and CD8+ T-cell responses in lymph nodes. Immunology and Cell Biology, 102 (4), pp.269-279. https://doi.org/10.1111/imcb.12740.

Persistent Link:
https://hdl.handle.net/11343/345462

Immunology & Cell Biology 2024; **102**: 269–279
www.wileyonlinelibrary.com/journal/icb

ORIGINAL ARTICLE

OPEN

The transcription factor SpiB regulates the fibroblastic reticular cell network and CD8$^+$ T-cell responses in lymph nodes

Harry L Horsnell[1], Wang HJ Cao[2,3,4], Gabrielle T Belz[2,3,4], Scott N Mueller[1,a] & Yannick O Alexandre[1,a]

1 Department of Microbiology and Immunology, University of Melbourne, Peter Doherty Institute for Infection and Immunity, Melbourne, VIC, Australia
2 Walter and Eliza Hall Institute of Medical Research (WEHI), Parkville, VIC, Australia
3 Department of Medical Biology, University of Melbourne, Parkville, VIC, Australia
4 University of Queensland Frazer Institute, University of Queensland, Brisbane, QLD, Australia

Keywords
CD8$^+$ T cells, fibroblastic reticular cells, immune response, lymph node, transcription factor

Correspondence
Scott N Mueller and Yannick O Alexandre, Department of Microbiology and Immunology, University of Melbourne, Peter Doherty Institute for Infection and Immunity, Melbourne, VIC, Australia.
E-mail: smue@unimelb.edu.au and yannick.alexandre@unimelb.edu.au

[a]Equal contributors.

Received 13 October 2023;
Revised 2 February 2024;
Accepted 14 February 2024

doi: 10.1111/imcb.12740

Immunology & Cell Biology 2024; **102**: 269–279

Abstract

Fibroblastic reticular cells (FRCs) construct microanatomical niches that support lymph node (LN) homeostasis and coordination of immune responses. Transcription factors regulating the functionality of FRCs remain poorly understood. Here, we investigated the role of the transcription factor SpiB that is expressed in LN FRCs. Conditional ablation of SpiB in FRCs impaired the FRC network in the T-cell zone of LNs, leading to reduced numbers of FRCs and altered homeostatic functions including reduced CCL21 and interleukin-7 expression. The size and cellularity of LNs remained intact in the absence of SpiB but the space between the reticular network increased, indicating that although FRCs were reduced in number they stretched to maintain network integrity. Following virus infection, antiviral CD8$^+$ T-cell responses were impaired, suggesting a role for SpiB expression in FRCs in orchestrating immune responses. Together, our findings reveal a new role for SpiB as an important regulator of FRC functions and immunity in LNs.

INTRODUCTION

Lymph nodes (LNs) are secondary lymphoid organs that form a network of tissues designed as a filtration and surveillance system. The microarchitecture of LNs is organized into distinct compartments with the primary goal of capturing and presenting antigens from peripheral tissues to cells of the immune system, generating immune responses.[1] Several types of nonhematopoietic stromal cells support the lymphoid architecture and function by constructing networks and defining compartments. CD31$^+$ lymphatic and blood endothelial cells build the vasculature of LNs required for the entry and exit of immune cells. Contractile pericytes expressing the adhesion molecule CD146 are also found in association with blood vessels. Fibroblastic reticular cells (FRCs) are the most prominent stromal cell population in LNs that form an interconnected cellular network that supports immune cell migration.[2] In addition, FRCs create a conduit system composed of extracellular matrix components and reticular fibers that facilitates the transport of lymph-derived antigens and signaling molecules, assisting in the induction of immune responses.[3] Inflammation transcriptionally reprograms

FRCs toward immune-related pathways that further support ongoing immune responses,[4–6] yet the role of FRC-specific transcription factors in controlling their function is unexplored.

Fibroblastic reticular cells comprise several subsets based on their intranodal location, markers and functions that all express podoplanin (PDPN). This heterogeneity in FRCs creates anatomical niches that support the homeostasis and support of immune responses in LNs.[7] Within the subcapsular sinus, marginal reticular cells (MRCs) and lymphatic endothelial cells form a unique niche for subcapsular macrophage development and homeostasis.[8–10] B-cell zone reticular cells (BRCs) include follicular dendritic cells (FDCs) and other CXCL13-expressing reticular cells that define this compartment and support humoral responses.[11] FDCs can arise from the differentiation of MRCs.[12] Within the T-cell zone, reticular cells [i.e. T-zone reticular cells (TRCs)] express the chemokines CCL19 and CCL21 that promote the attraction and retention of T cells and DCs that express CCR7 and produce cytokines such as interleukin (IL)-7 that are critical for T-cell survival.[13,14] In addition, MRCs, BRCs and TRCs are all characterized by the high expression of the bone marrow stromal cell antigen-1, or CD157. Conversely, in the medulla, $CD157^{low}$ FRCs (medRC) were recently shown to support plasma cells by providing IL-6.[7,15] Finally, adventitial reticular cells (ARCs) that express CD34 and Ly6C form a specific niche by surrounding blood vessels and may function as precursors of adult FRCs.[16,17]

LN FRCs develop from fibroblast activation protein-α^+ lymphoid tissue organizer cells of mesenchymal origin.[18] Their development requires sequential differentiation and maturation steps that are not fully understood. Several pathways including lymphotoxin-β receptor signaling, nuclear factor-kappa B and effectors of Hippo signaling, YAP and TAZ, were shown to instruct the maturation of FRCs from precursor cells.[19–22] Deficiency in these pathways results in a reduction in the cellularity of FRCs and these immature FRCs harbor lower expression of the homeostatic chemokines CCL19, CCL21 and CXCL13 as well as reduction in IL-7. Interestingly, immature FRCs still produce reticular fibers and a functional conduit network in LNs, but the overall size and cellularity of the tissue are decreased.[19,20] These defects in the FRC network also resulted in impaired $CD8^+$ T-cell responses during viral infections, indicating that the generation of optimal immune responses require a functional and healthy FRC network.[19,20] Surprisingly, despite the diversity of signaling pathways that regulate FRC function, little is known about how transcription factors engage in controlling FRC biology.

We previously identified the transcription factor SpiB as a regulator of FRC maturation in the spleen.[17,23] Here, we investigated the role of SpiB in LN homeostasis and immune responses. We found that SpiB expression is conserved in LN FRCs and conditional ablation of SpiB expression impacted the cellularity and functionality of the FRC network in the T-cell zone at steady state. Deletion of SpiB in FRCs did not affect LN tissue size or homeostasis of immune cells but impacted T-cell priming following viral infection. These data indicate conserved function of the transcription factor SpiB in lymphoid organ FRCs for the induction of pathogen-specific T-cell responses.

RESULTS

The transcription factor SpiB is expressed by lymph node FRCs

We previously identified a role for SpiB in FRCs in the spleen.[17] We first sought to determine whether SpiB expression was conserved in LNs. Integration of single cell RNA-sequencing data sets analyzing FRCs from both spleen and LNs revealed expression of *Spib* messenger RNA in FRCs from LN B and T-cell zones as well as medullary reticular cells (medRCs) but low to no expression in LN ARCs or pericytes (Supplementary figure 1a). BRCs had higher expression of *Spib* compared with TRCs. We then used SpiB-tdTomato reporter mice to examine expression in LN stromal cells by flow cytometry and observed that FRCs and lymphatic endothelial cells had the highest levels of tdTomato while blood endothelial cells and pericytes had low expression (Figure 1a, b). We then used a new gating strategy to further define FRC subsets in LNs. We identified $CD21/35^+$ FDC, $MadCAM1^+$ MRCs, $CD157^+$ TRC, $Ly6C^+CD157^-$ ARCs and $Ly6C^-CD157^-$ medRCs (Figure 1c).[15,17,24] Flow cytometry analysis revealed that FDCs and MRCs had the highest expression of tdTomato followed by TRC, while ARC and medRC had low levels of tdTomato (Figure 1d).

The transcription factor SpiB supports FRC homeostasis

To investigate a role for SpiB in LN FRCs, we used Ccl19-Cre/$SpiB^{flox/flox}$ mice ($SpiB^{\Delta CCL19}$) as previously described[17] and confirmed the absence of *Spib* in sorted populations of TRCs, ARCs and medRCs by qPCR (Supplementary figure 1b). We observed a significant reduction in the numbers of FRCs, lymphatic endothelial cells and blood endothelial cells but not of pericytes in the LN of $SpiB^{\Delta CCL19}$ mice (Figure 2a). The reduction in

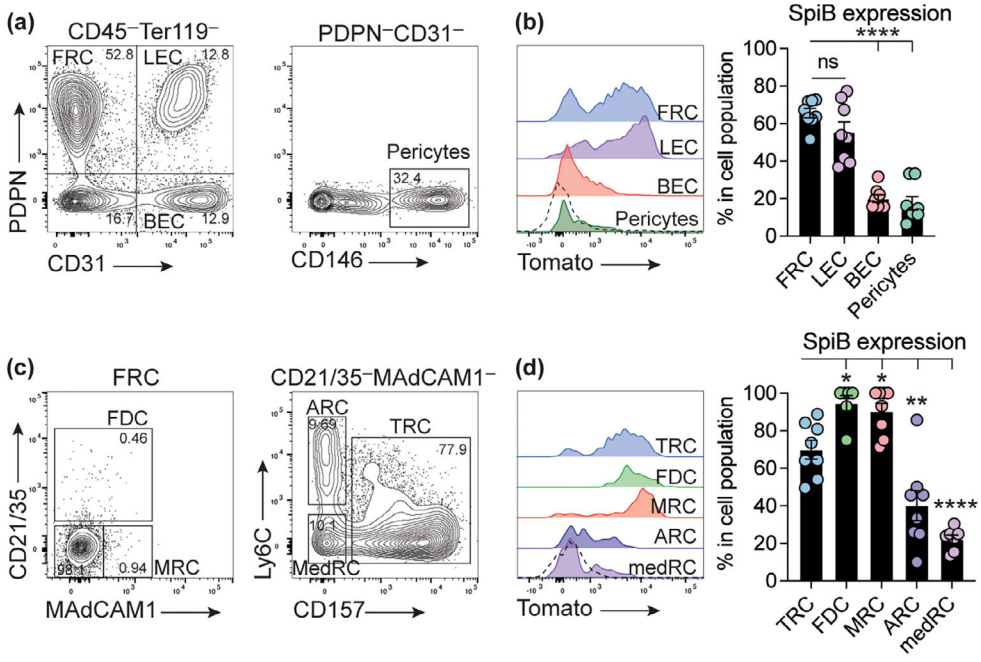

Figure 1. LN FRCs express the transcription factor SpiB. **(a)** Gating strategy to identify LN stromal cells by flow cytometry. Hematopoietic cells were excluded, and stromal cells were identified with the markers PDPN, CD31 and CD146. **(b)** Flow cytometry of LN stromal cell subsets in SpiB-TdTomato mice. Representative histograms of SpiB expression (left) and pooled data (means ± standard error of the mean) from eight mice combined from three independent experiments. Dotted line represents baseline fluorescence from WT control. **(c)** Gating strategy to identify LN FRC subsets by flow cytometry. **(d)** Flow cytometry of LN stromal cell subsets in SpiB-TdTomato mice. Representative histograms of SpiB expression (left) and pooled data (means ± standard error of the mean) from eight mice combined from three independent experiments. Dotted line represents baseline fluorescence from WT control. $*P < 0.05$, $**P < 0.01$, $****P < 0.0001$. ns, nonsignificant, by analysis of variance with Tukey's multiple comparisons test **(b, d)**. ARC, adventitial reticular cell; BEC, blood endothelial cell; FDC, follicular dendritic cell; FRC, fibroblastic reticular cell; LEC, lymphatic endothelial cell; LN, lymph node; MedRC, medullary reticular cell; MRC, marginal reticular cell; PDPN, podoplanin; TRC, T-zone reticular cell; WT, wild type.

lymphatic endothelial cells and blood endothelial cells may reflect a bystander effect because endothelial cells are not targeted in CCL19-Cre mice.[20,25] Among FRC subsets, TRCs and MRCs were reduced in cellularity in SpiB$^{\Delta CCL19}$ mice, but FDCs, ARCs and medRCs were not changed (Figure 2b). Thus, expression of SpiB was required for maintenance of the stromal cell networks that support defined areas of LNs.

We previously showed that in the absence of SpiB, splenic TRCs had increased expression of genes expressed by ARCs, notably the stem marker CD34, and decreased expression of mature TRC markers, including *Il7*, *Ccl19* and *Grem1*, which indicated a role for SpiB in supporting the differentiation of spleen TRCs from adventitial precursor cells.[17] We did not observe changes in *Ccl19* expression in SpiB-deficient LN TRCs (Supplementary figure 1c); however, the expression of the homeostatic cytokine *Il7* was significantly reduced in FRC subsets and *Grem1* expression was reduced in TRCs (Figure 2c). Expression of *Cd34* remained low in TRCs and expression of the immature genes *Cspg4* and *Mfge8* were not changed in the absence of SpiB (Supplementary figure 1c). This suggests that SpiB likely regulates distinct aspects of the differentiation of FRCs in LNs. We then asked whether SpiB regulates the expression of other canonical markers in FRCs, including the proteins PDPN, CD157, VCAM-1 and CD140a (PDGFRa). We observed small changes in expression of these markers in MRCs in the absence of SpiB and no differences among other LN FRC subsets except for CD140a that was also slightly reduced in LN TRCs (Supplementary figure 1d). In addition, SpiB$^{\Delta CCL19}$ FRCs demonstrated normal expression of the chemokines *Ccl2*, *Ccl7*, *Cxcl9*, *Cxcl10*, *Cxcl12*, *Cxcl13* and the alarmin *Il33*, except for a reduction of *Ccl7* expression in TRCs and *Cxcl13* in medRC (Supplementary figure 1e). We observed a significant reduction in intracellular CCL21 expression in SpiB$^{\Delta CCL19}$ FRCs, particularly within TRCs, and no

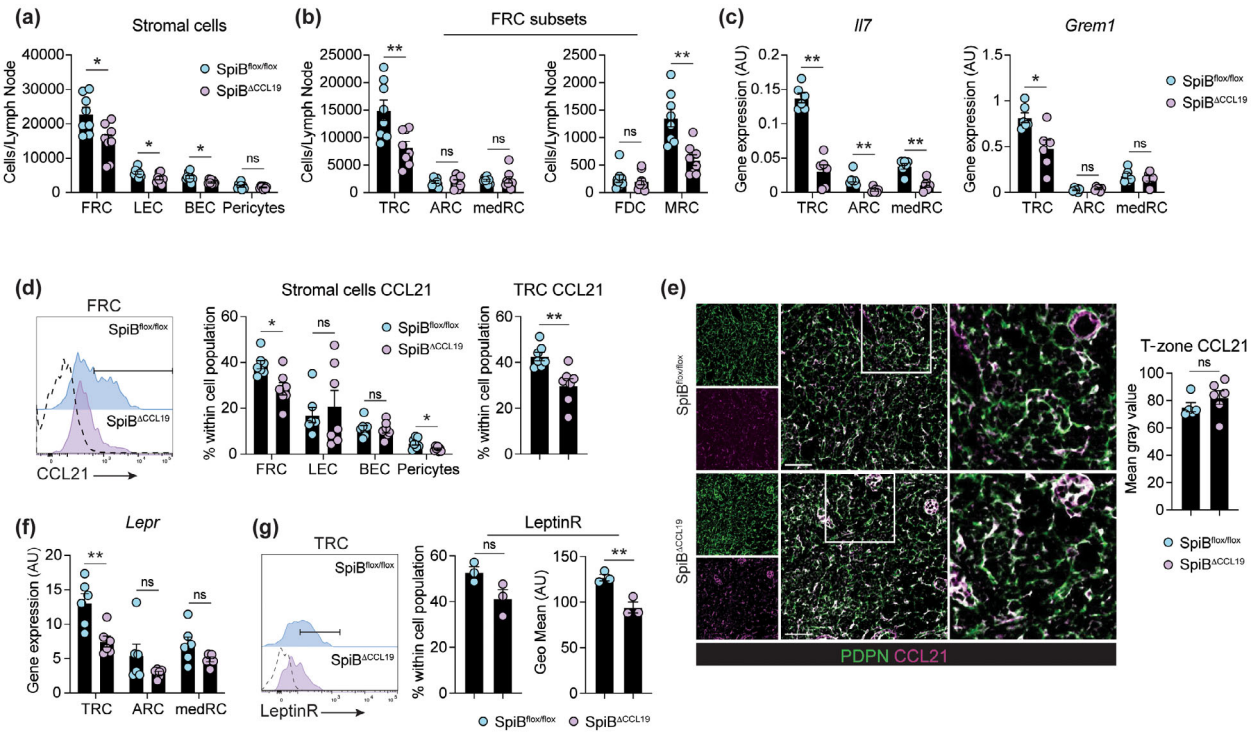

Figure 2. The transcription factor SpiB controls the T-zone reticular cell network and functionality. **(a, b)** Enumeration of LN stromal cells and FRC subsets from control SpiB$^{flox/flox}$ and SpiB$^{\Delta CCL19}$ mice by flow cytometry. Graphs show pooled data (means ± standard error of the mean) from two independent experiments with eight mice per group. **(c)** Analysis of *Il7* and *Grem1* expression in LN-sorted TRCs, ARC and medRC of control SpiB$^{flox/flox}$ and SpiB$^{\Delta CCL19}$ mice by qPCR. $n = 6$ mice from three independent sorts. **(d)** Flow cytometry analysis and representative histograms (left) of intracellular CCL21 expression in FRCs from control SpiB$^{flox/flox}$ and SpiB$^{\Delta CCL19}$ mice. Fluorescence minus one staining is shown by the histogram with a dotted line and used to discriminate CCL21$^+$ from CCL21$^-$ cells. Percentage (right) of CCL21$^+$ stromal cell subsets and TRCs in the LNs of control SpiB$^{flox/flox}$ and SpiB$^{\Delta CCL19}$ mice. Graphs show pooled data (means ± standard error of the mean) from two independent experiments with seven mice per group. **(e)** Skin-draining LN sections from control SpiB$^{flox/flox}$ and SpiB$^{\Delta CCL19}$ mice were stained for PDPN and CCL21 and analyzed by confocal microscopy, and the area of CCL21 was quantified in the T-cell zone of LN. Graph shows pooled data (means ± standard error of the mean) from two independent experiments with five and six mice per group. Scale bar, 50 μm. **(f)** Analysis of *Lepr* expression in LN-sorted TRCs, ARC and medRC of control SpiB$^{flox/flox}$ and SpiB$^{\Delta CCL19}$ mice by qPCR. $n = 6$ mice from three independent sorts. **(g)** Flow cytometry analysis of LepR expression in TRCs from control SpiB$^{flox/flox}$ and SpiB$^{\Delta CCL19}$ mice. Left: representative histograms of LepR staining with fluorescence minus one staining shown as dotted line and used to discriminate LepR$^+$ from LepR$^-$ cells. Right: graphs show the percentage of LepR$^+$ TRCs in LNs and the mean fluorescence intensity (GeoMean) of LepR in TRCs. Data are representative of one experiment out of two, with three mice per group. $*P < 0.05$, $**P < 0.01$, ns, nonsignificant, by the unpaired two-tailed *t*-test **(a, b, g)** and the Mann–Whitney *U*-test **(c–f)**. ARC, adventitial reticular cell; BEC, blood endothelial cell; FRC, fibroblastic reticular cell; LEC, lymphatic endothelial cell; LN, lymph node; MRC, marginal reticular cell; PDPN, podoplanin; qPCR, quantitative polymerase chain reaction; TRC, T-zone reticular cell.

changes in ARCs and medRCs (Figure 2d; Supplementary figure 1f). The absence of SpiB also did not affect CCL21 expression in endothelial cells or pericytes (Figure 2d). Histological examination showed no difference in CCL21 deposition in the T-cell zone of SpiB$^{\Delta CCL19}$ mice (Figure 2e), possibly because of accumulation of the chemokine on the reticular network via heparan sulfate binding.[26] LN FRCs that surround high endothelial venules and lymphatic endothelial cells also predominantly express the leptin receptor (LepR), which might promote FRC survival and functions.[27] We found that *Lepr* was reduced in TRCs in the absence of SpiB and confirmed the decrease of LepR expression by flow cytometry in SpiB-deficient TRCs (Figure 2f, g). Overall, these data show that SpiB regulates the maintenance of TRCs and MRCs in LNs and regulates discreet components of FRC function.

Normal lymph node architecture in mice lacking SpiB in FRCs

As FRCs play crucial roles in regulating LN homeostasis, we investigated whether the reduction in numbers of TRCs and altered functionality impacted immune cell cellularity

and the LN architecture. The loss of SpiB in FRCs resulted in a small but nonsignificant decrease in total LN cellularity, composed of small but nonsignificant changes in the numbers of B cells, $CD4^+$ and $CD8^+$ T cells (Figure 3a; Supplementary figure 2a). We observed a small but nonsignificant reduction in $CD44^-CD62L^+$ naïve and $CD44^+CD62L^+$ central memory $CD8^+$ T cells in the LN of $SpiB^{\Delta CCL19}$ mice (Supplementary figure 2a, b). We also found a nonsignificant decrease in naïve $CD44^-CD62L^+$ $CD4^+$ T-cell cellularity but not $CD44^+CD62L^-$ activated $CD4^+$ T cells, corresponding to a small but significant reduction in the percentage of naïve $CD4^+$ T cells and an increase in activated $CD4^+$ T cells in $SpiB^{\Delta CCL19}$ mice (Supplementary figure 2a, b). Among B cells, IgM^+ and IgD^+ subsets were unchanged in $SpiB^{\Delta CCL19}$ mice (Supplementary figure 2a, b). Other immune cells

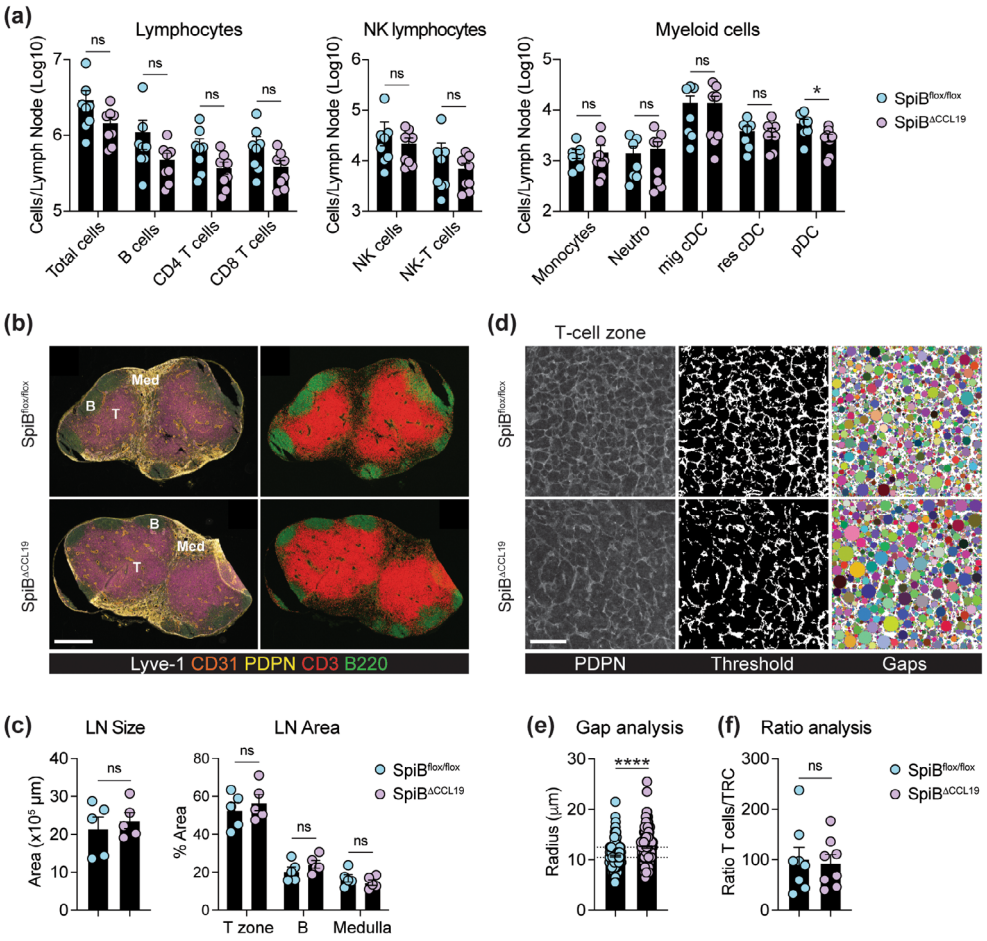

Figure 3. SpiB deletion in FRC does not impact immune cell homeostasis or LN architecture. **(a)** Enumeration of immune cells from control $SpiB^{flox/flox}$ and $SpiB^{\Delta CCL19}$ mice by flow cytometry. Graphs show pooled data (means ± standard error of the mean) from two independent experiments with seven and eight mice per group. **(b)** Skin-draining LN sections from control $SpiB^{flox/flox}$ and $SpiB^{\Delta CCL19}$ mice were stained for Lyve-1, CD31, PDPN, CD3 and B220 and analyzed by confocal microscopy. Left images display the merged staining and right images the merged staining of CD3 and B220 only. Scale bar, 500 µm. **(c)** Quantification of the total LN size area (left graph) and LN compartment areas (right graph). Graphs show pooled data (means ± standard error of the mean) from two independent experiments with five mice per group. **(d, e)** TRC gap analysis on LN sections from control $SpiB^{flox/flox}$ and $SpiB^{\Delta CCL19}$ mice. Sections were stained for PDPN (left) and converted to threshold images (middle) and overlayed with circles for gap analysis (right). Graph shows the quantification of circle radius. Each point represents a circle radius and data are pooled from two independent experiments with five mice per group. Scale bar, 50 µm. **(f)** Ratio analysis of total T cells versus TRCs in control $SpiB^{flox/flox}$ and $SpiB^{\Delta CCL19}$ mice. Graph shows pooled data (means ± standard error of the mean) from two independent experiments with eight mice per group $^*P < 0.05$, $^{****}P < 0.0001$, ns, nonsignificant, by the Mann–Whitney *U*-test **(a, c, e, f)**. cDC, conventional dendritic cell; FRC, fibroblastic reticular cell; LN, lymph node; NK, natural killer; pDC, plasmacytoid dendritic cell; PDPN, podoplanin; TRC, T-zone reticular cell.

including NK and NK-T cells, monocytes, neutrophils and dendritic cell subsets, apart from plasmacytoid dendritic cells, were not altered in the LNs of SpiB$^{\Delta CCL19}$ mice (Figure 3a; Supplementary figure 2a, c).

The gross architecture and total surface area of LNs remained unchanged in SpiB$^{\Delta CCL19}$ mice (Figure 3b, c; Supplementary figure 2d). The absence of SpiB expression in FRCs also did not affect the organization or size of the LN T-cell zone, B-cell follicles or medulla (Figure 3c). However, a closer examination of the PDPN^{+} TRC network in the T-cell zone revealed that the TRC network was less dense in SpiB$^{\Delta CCL19}$ mice (Figure 3d). Quantification of the spacing between FRCs in the T-cell zone network using gap analysis confirmed that the space between the reticular network fibers was increased in the absence of SpiB (Figure 3e). The reduction in FRCs and lymphocyte cellularity resulted in maintenance of the ratio of T cells to TRCs (Figure 3f). Thus, increased spacing between TRCs in LNs from SpiB$^{\Delta CCL19}$ mice occurred in the absence of a reduction in tissue size, suggesting that the FRC network stretched to maintain T-cell homeostasis.

SpiB expression enables FRC to regulate T-cell immunity

Having identified a role for SpiB in regulating the TRC function and network properties at homeostasis, we then investigated whether SpiB expression in FRCs supports immune responses. For this, we labeled with CellTrace Violet gBT-I CD8^{+} T cells specific for a herpes simplex virus (HSV) glycoprotein B epitope and transferred them into SpiB$^{\Delta CCL19}$ and control mice followed by subcutaneous HSV-1 KOS infection (Figure 4a). We tracked CD45.1^{+} gBT-I CD8^{+} T cells in the draining popliteal LNs of infected mice (Figure 4b). Proliferation of gBT-I CD8^{+} T cells 3 days after infection was diminished in SpiB$^{\Delta CCL19}$ mice, reflected by a lower average number of divisions (proliferation index) and reduced fold expansion (replication index) among dividing cells (Figure 4b, c). Accumulation of divided gBT-I CD8^{+} T cells required SpiB expression in FRCs (Figure 4d), yet upregulation of the activation markers CD69 and CD25 by gBT-I cells was unaffected, suggesting normal differentiation of the CD8^{+} T cells that entered division (Figure 4e).

We then explored whether the reduced early proliferation of gBT-I cells would further impact their effector functions. For this, we similarly tracked and analyzed the differentiation of gBT-I cells into short-lived effector cells and memory precursor effector cells based on the expression of KLRG1 and the IL-7R, respectively, in the draining popliteal LNs of infected mice 8 days after infection (Figure 4f, g). Although total numbers of CD8^{+} T, CD4^{+} T and B cells were similar in LNs of SpiB$^{\Delta CCL19}$ mice when compared with littermate control mice, we observed a significant reduction in numbers of virus-specific gBT-I CD8^{+} T cells (Figure 4h). The differentiation of gBT-I cells into short-lived effector cells and memory precursor effector cells was not affected (Figure 4i), and induction of GL7^{+}CD38^{-} germinal center B cells, CD138^{+} antibody-secreting cells and CXCR5^{+}PD-I^{+} T_{FH} cells was not altered in the LNs of HSV-1–infected SpiB$^{\Delta CCL19}$ mice (Supplementary figure 3a, b). This suggested that SpiB expression in FRCs preferentially supported CD8^{+} T-cell responses. To confirm this, we infected mice with lymphocytic choriomeningitis virus and examined cellularity in inguinal LNs. Expansion of endogenous CD4^{+} and CD8^{+} T cells and virus-specific transgenic P14 CD8^{+} T cells was reduced in SpiB$^{\Delta CCL19}$ mice, but differentiation of effector CD8^{+} T cells was not altered (Supplementary figure 2c, d).

Finally, we observed significantly fewer TRCs in SpiB$^{\Delta CCL19}$ mice during the course of HSV-1 infection that resulted in a significant increase in the ratio of total T cells to TRCs in LNs (Figure 4j; Supplementary figure 3e). The decrease in the TRC network was likely not because of a defect in their proliferation as we did not observe changes in Ki-67 expression in SpiB$^{\Delta CCL19}$ mice, nor an increase in apoptosis because FRCs had high expression of the prosurvival protein BCL-2 (Supplementary figure 3f, g). The expansion and organization of the LN T-cell zone, B-cell follicles or medulla were also not affected by the absence of SpiB (Supplementary figure 3h, i). However, analysis of the PDPN^{+} TRC network revealed that the increase of space between the reticular network was maintained in the absence of SpiB following HSV infection (Figure 4k, l). These results suggest that SpiB expression in FRCs is critical for the expansion of the FRC network that parallels and regulates the early priming and proliferation of CD8^{+} T cells during viral infection. Together, our findings expand our understanding of the role of SpiB in regulating the LN FRC network and a crucial role in supporting the induction of CD8^{+} T-cell responses.

DISCUSSION

This study identified the transcription factor SpiB as a regulator of FRC homeostasis and functionality in LNs. We found that in the absence of SpiB, FRCs were decreased in cellularity and key homeostatic factors expressed by FRCs such as CCL21 and *Il7* were reduced. However, we found that the size and architecture of LNs

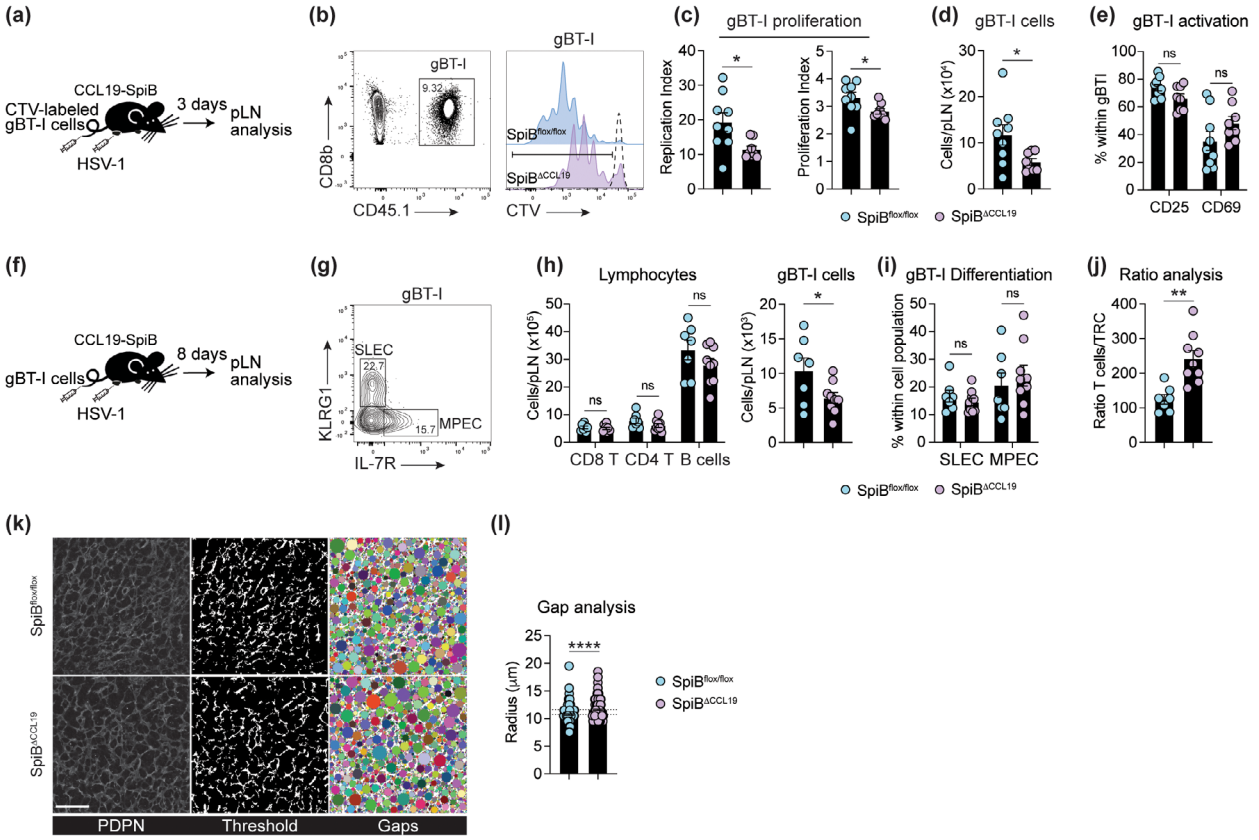

Figure 4. SpiB expression in FRC regulates T-cell responses during viral infection. **(a)** Experimental schematic of HSV-1 infection for T-cell priming. Mice were injected with 1.5 × 10^6 CTV-labeled gBT-I cells and 24 h later infected subcutaneously in the footpad with HSV-1. Draining popliteal LNs were analyzed 3 days after infection. **(b)** Flow cytometry analysis of CD45.1$^+$ CD8$^+$ gBT-I cells and representative histograms of CTV-labeled gBT-I cells in the draining popliteal LN of control SpiB$^{flox/flox}$ and SpiB$^{\Delta CCL19}$ mice, 3 days after subcutaneous HSV-1 infection. Dotted histogram represents CTV staining on gBT-I cells from naïve mice used to gate on divided gBT-I cells. **(c–e)** Quantification of gBT-I cell expansion and activation. **(c)** The left graph shows the replication index (calculated as the total number of divided cells/cells that went into division) and the right graph shows the proliferation index (calculated as the total number of divisions/cells that went into division) of gBT-I cells in the draining popliteal LN of control SpiB$^{flox/flox}$ and SpiB$^{\Delta CCL19}$ mice. **(d)** The graph shows the enumeration of divided gBT-I cells, 3 days after subcutaneous HSV-1 infection. **(e)** Quantification of the percentage of CD25$^+$ and CD69$^+$ gBT-I cells. Graphs show pooled data (means ± standard error of the mean) from two independent experiments with nine and eight mice per group. **(f)** Experimental schematic of HSV-1 infection. Mice were injected with 5 × 10^4 gBT-I cells and 24 h later infected subcutaneously in the footpad with HSV-1. Draining popliteal LNs were analyzed 8 days after infection. **(g–i)** Flow cytometry analysis of CD45.1$^+$ gBT-I cells in the draining popliteal LN, 8 days after subcutaneous HSV-1 infection. **(g)** Short-lived effector cells (SLECs) and memory precursor effector cells (MPECs) gBT-I cells were identified as KLRG1$^+$ and IL-7R$^+$, respectively. Enumeration of **(h)** lymphocytes and gBT-I cells and **(i)** gBT-I cell differentiation in the draining popliteal LN of control SpiB$^{flox/flox}$ and SpiB$^{\Delta CCL19}$ mice, 8 days after subcutaneous HSV-1 infection. **(j)** Ratio analysis of total T cells versus TRCs in control SpiB$^{flox/flox}$ and SpiB$^{\Delta CCL19}$ mice in the draining popliteal LN, 8 days after subcutaneous HSV-1 infection. Graphs **(h, j)** show pooled data (means ± standard error of the mean) from two independent experiments with seven and nine mice per group. **(k, l)** TRC gap analysis on LN sections from control SpiB$^{flox/flox}$ and SpiB$^{\Delta CCL19}$ mice at day 8 post-HSV infection. The graph shows the quantification of circle radius. Each point represents a circle radius and data are pooled from two independent experiments with five mice per group. Scale bar, 50 μm. *$P < 0.05$, **$P < 0.01$, ****$P < 0.0001$, ns, nonsignificant, by the unpaired two-tailed *t*-test **(c–e, l)** or the Mann–Whitney *U*-test **(h–j)**. CTV, CellTrace Violet; FRC, fibroblastic reticular cell; HSV, herpes simplex virus; IL, interleukin; LN, lymph node; MPEC, memory precursor effector cell; PDPN, podoplanin; pLN, popliteal lymph node; SLEC, short-lived effector cell; TRC, T-zone reticular cell.

were not affected. In addition, we found that the absence of SpiB expression in FRCs did not affect the expression of canonical FRC markers such as PDPN, CD140a, BST1 and VCAM1, or the expression of other chemokines, including *Ccl19*, suggesting normal differentiation of FRCs from precursor cells. This is in contrast to previous

work that identified that the lymphotoxin beta signaling pathway or the expression of YAP/TAZ in CCL19$^+$ FRCs is critical for the maturation of FRCs from precursor cells required for proper organization of LN structures.[19–21] In these models, homeostatic chemokine expression such as CCL21 and CCL19 was also strongly reduced in FRCs that impacted the recruitment of immune cells, leading to smaller LN size and deformed architecture, notably the delineation of the T- and B-cell compartments. We found that even though CCL21 expression was reduced in FRCs in the absence of SpiB, our histological examination of LNs showed normal CCL21 accumulation on the reticular network, suggesting that reduced chemokine expression in FRCs might be compensated from other sources such as endothelial cells, which are a source of the chemokine in lymphoid tissues.[5,14] In addition, intact expression of *Ccl19* in our model might support the recruitment and positioning of lymphocytes within LNs and its normal compartmentalization.

Despite normal compartmentalization of the LN, we observed that the space between the reticular network fibers within the T-cell zone of LNs was increased in the absence of SpiB expression. This implies that the FRC network has remodeled to maintain the size of the LN and ratio with T cells in the steady state. Under basal conditions, FRCs maintain tension via PDPN expression that facilitates the contraction of the actomyosin cytoskeleton[28,29] and this contraction of the FRC network regulates the stiffness of the LN as well as their size. During the first few days of an immune response, CLEC-2 expression from mature dendritic cells engages and blocks PDPN functions and downstream signaling to relax the actomyosin cytoskeleton and induce the stretching of FRCs.[28,29] This regulates LN tension to accommodate the increase of cellularity because of lymphocyte recruitment.[30–32] We did not find that SpiB regulates PDPN expression in FRCs, suggesting that additional molecules involved in FRC contractility should be investigated in our model. A recent report identified that the PDPN-binding partner surface proteins CD44 and CD9 suppress PDPN functions and the contractility of FRCs.[33] Whether SpiB regulates expression of both CD44 and CD9 or regulates the tension of the TRC network remains to be addressed.

Our data identified that SpiB expression in FRCs is required for the optimal activation of naïve CD8$^+$ T cells during viral infection. In the absence of SpiB, the early proliferation of antiviral CD8$^+$ T cells was delayed. This corroborates our previous findings where we identified a role for SpiB expression in spleen FRCs in regulating CD8 T-cell responses to acute and chronic systemic viral infection.[17] Previous studies also identified a defect in CD8$^+$ T-cell responses when the FRC network was impaired in the absence of the lymphotoxin beta signaling pathway or the expression of YAP/TAZ in FRCs.[19,20] In these two studies, the decrease of FRC as well as reduction in homeostatic chemokine expression resulted in a paucity of immune cells in LNs, and disorganized T/B segregation that likely contributed to the reduced T-cell response. Similarly, gradual depletion of the CCL19$^+$ FRC network revealed that the topology of the network can accommodate up to 50% decrease before affecting immune cell recruitment to LNs, intranodal cell motility or priming of CD8$^+$ T cells.[34] Here we found that deletion of SpiB expression in FRCs led to an approximate 50% reduction in TRC numbers and altered spacing of the TRC network at steady state. This disadvantage persisted during virus infection, resulting in an increased ratio of T cells to TRCs, suggesting that T cells might make fewer contacts with FRCs as the LN expands. This could, at least in part, explain impaired T-cell priming following virus infection of SpiB$^{\Delta CCL19}$ mice. However, we do not rule out additional functional programming of TRCs by SpiB. In support of this, we found reduced expression of CCL21, *Il7* and LepR in SpiB-deficient TRCs. Two recent studies found that FRC numbers were reduced in LNs from mice lacking LepR.[27,35] Future studies would need to uncouple the role of SpiB in regulating FRC cellularity and FRC cellular physiology during inflammation to determine factors that influence immune responses beyond providing the framework required for optimal T–DC interactions. Interestingly, SpiB is also expressed in human FDCs and TRCs, suggesting potential conserved functions across species.[36] In summary, our study establishes a role for the transcription factor SpiB in regulating distinct LN FRC functions and provides new insights into how the FRC network supports immune responses.

METHODS

Mice

C57BL/6, CCL19-Cre, SpiB$^{flox/flox}$, gBT-I3B6.SJL-PtprcaPep3b/BoyJ (gBT-I.CD45.1) and P143B6.SJL-PtprcaPep3b/BoyJ (P14.CD45.1) mice were bred in the Doherty Institute. SpiB-tdTomato were bred at the Walter and Eliza Hall Institute of Medical Research. SpiB$^{\Delta CCL19}$ mice were generated by crossing CCL19-Cre and SpiB$^{flox/flox}$ mice. Animal experiments were approved by the University of Melbourne Animal Ethics Committee. Mice were maintained under specific pathogen–free conditions and housed in individually ventilated cages. All mice were sex- and age-matched, and both female and male mice were used between 8 and 14 weeks of age.

Adoptive transfer of transgenic CD8$^+$ T cells

Recipient mice were intravenously injected with 5×10^4 gBT-I or P14 cells 24 h before infection. For priming experiments, gBT-I cells were first labeled with CellTrace Violet (ThermoFischer) at a final concentration of 5 μM according to manufacturer's instructions and 1.5 million cells were intravenously injected in recipient mice.

Virus and infections

Herpes simplex virus-1 KOS strain and lymphocytic choriomeningitis virus Armstrong strain were used in this study. Mice were anesthetized with a mixture of ketamine/xylazine at 100 and 20 mg kg^{-1}, respectively, and infected subcutaneously in the footpad with 2×10^4 of plaque-forming units of HSV-1. Mice were infected intraperitoneally with 2×10^5 plaque-forming units of LCMV Armstrong.

LN digestion and flow cytometry

Lymph nodes were incubated at 37°C in Roswell Park Memorial Institute medium with 2 mg mL^{-1} collagenase D (Roche), 0.8 mg mL^{-1} dispase (ThermoFischer) and 100 μg mL^{-1} DNase (Sigma) and 2% fetal bovine serum. LNs were gently digested by removing and replacing the cell suspension every 10 min until completely digested. LN cell suspensions were resuspended in fluorescence-activated cell sorting buffer [phosphate-buffered saline (PBS) 2% bovine serum albumin 5 mM ethylenediaminetetraacetic acid] and filtered through 70 μM before antibody staining. Cells were stained in fluorescence-activated cell sorting buffer containing CD16/32 Fc blocking antibody for 30 min at 4°C. Antibodies used for staining are detailed in Supplementary table 1. Intracellular staining for CCL21 was performed using eBioscience Intracellular Fixation & Permeabilization Buffer Set according to the manufacturer's instructions. Cells were enumerated by adding SPHERO calibration particles (BD) to each sample before acquisition on flow cytometer and samples were acquired using FACSFortessa (BD) or Cytek Aurora. FlowJo software (V10) was used for analysis.

Quantitative real-time PCR

Total RNA was extracted from sorted samples using RNeasy Plus Micro Kit (Qiagen) and converted to complementary DNA using the High Capacity cDNA Reverse Transcription Kit (Thermo Fisher Scientific) according to the manufacturer's instructions. Genes of interest were preamplified from complementary DNA using TaqMan PreAmp Master Mix (Thermo Fisher Scientific) and samples were analyzed by real-time qPCR using Fast SYBR Green Master Mix (Thermo Fisher Scientific). Cycle-threshold values were determined for genes individually, and gene expression was normalized to the housekeeping genes *Hprt* and *Gapdh* (ΔCt) and presented as $2^{-\Delta Ct}$ (arbitrary units). Details of the primers can be found in Supplementary table 2.

Immunofluorescence and confocal imaging

LNs were harvested and fixed in 4% paraformaldehyde (Electron Microscopy Sciences) for 4 h, incubated in 30% sucrose and embedded in OCT freezing media (Trajan Scientific). Control and SpiB$^{\Delta CCL19}$ LNs were embedded in the same block for comparative analysis. Tissue sections were cut at 20-μm thickness with a cryostat (Leica CM3050S). Sections were blocked for 2 h (10% normal donkey serum + 0.3% Triton X-100 in PBS) at room temperature. Sections were then stained with primary antibodies (Supplementary table 1) overnight at 4°C (diluted in PBS, 10% normal donkey serum and 0.01% Triton X-100). Sections were washed in PBS–Tween 0.05% three times for 15 min and then blocked at room temperature for 2 h. Secondary antibodies (Supplementary table 1) were applied for 2 h at room temperature (diluted in PBS, 10% normal serum and 0.01% Triton X-100). This was followed by two 15-min washes of PBS–Tween 0.05% and a final wash of 15 min in PBS. Sequential staining and blocking of CCL21 (goat) and PDPN (hamster) were performed to prevent cross reactivity. Stained sections were mounted in ProLong Gold antifade reagent (Thermo Fisher Scientific) and images were acquired on an LSM980 confocal microscope (Carl Zeiss). Image analysis was performed in ImageJ. *Quantification of CCL21 and LN architecture*. Hand-drawn regions of interest of the LN were used to calculate the LN area. T- and B-cell zones and the medullary area were calculated using the CD3-, B220- and LYVE-1-positive–stained region on maximum projections. T-cell zone FRC regions of interest were used to generate PDPN masks that were applied to CCL21 staining to calculate the fluorescent intensity within the fibroblast network.

Gap analysis. The FRC gap analysis used a MATLAB script from the Acton lab.[30] PDPN fluorescence maximum projections were converted into a binary mask before a circle-fitting algorithm consecutively fit the largest circle possible within the gaps in the network that did not overlap with other fitted circles. Each circle was given a radius. The top 10 largest radii from each regions of interest were plotted.

Statistical analysis

Graphs and statistics were generated using Prism 9 (GraphPad). Samples were tested for normality, and two groups were compared using the two-tailed Mann–Whitney *U*-test or the unpaired *t*-test. Multiple groups were analyzed with one-way analysis of variance, followed by Tukey's post-test comparison or Kruskal–Wallis, based on Gaussian distribution. All graphs depict means ± standard error of the mean. Details of statistical analysis are indicated in the figure captions and include the statistical test used. ns indicates nonsignificance; $*P < 0.05$, $**P < 0.01$, $***P < 0.001$ and $****P < 0.0001$.

ACKNOWLEDGMENTS

We thank the Bioresources Facility and the Melbourne Cytometry Platform at the Peter Doherty Institute for technical support. Confocal Imaging was performed at the Biological Optical Microscopy Platform (BOMP) Facility at The University of Melbourne. Open access publishing is facilitated by The University of Melbourne, as part of the Wiley - The University of Melbourne agreement via the Council of Australian University Librarians.

AUTHOR CONTRIBUTIONS

Harry L Horsnell: Funding acquisition; investigation; methodology; visualization; writing – review and editing. **Wang HJ Cao:** Resources. **Gabrielle T Belz:** Resources. **Scott N Mueller:** Conceptualization; funding acquisition; supervision; writing – review and editing. **Yannick O Alexandre:** Conceptualization; funding acquisition; investigation; methodology; supervision; writing – original draft; writing – review and editing.

CONFLICT OF INTEREST

The authors declare that they have no competing interests.

FUNDING INFORMATION

This work was supported by the Australian Research Council (DP230102108 to SNM and YOA) and the National Health and Medical Research Council (Senior Research Fellowship 2017220 to SNM). HLH is supported by an EMBO Postdoctoral Fellowship ALTF 776-2022.

DATA AVAILABILITY STATEMENT

The data that support the fundings of this study are available from the corresponding authors upon reasonable request.

REFERENCES

1. Alexandre YO, Mueller SN. Stromal cell networks coordinate immune response generation and maintenance. *Immunol Rev* 2018; **283**: 77–85.
2. Bajenoff M, Egen JG, Koo LY, *et al*. Stromal cell networks regulate lymphocyte entry, migration, and territoriality in lymph nodes. *Immunity* 2006; **25**: 989–1001.
3. Acton SE, Onder L, Novkovic M, Martinez VG, Ludewig B. Communication, construction, and fluid control: lymphoid organ fibroblastic reticular cell and conduit networks. *Trends Immunol* 2021; **42**: 782–794.
4. Gregory JL, Walter A, Alexandre YO, *et al*. Infection programs sustained lymphoid stromal cell responses and shapes lymph node remodeling upon secondary challenge. *Cell Rep* 2017; **18**: 406–418.
5. Malhotra D, Fletcher AL, Astarita J, *et al*. Transcriptional profiling of stroma from inflamed and resting lymph nodes defines immunological hallmarks. *Nat Immunol* 2012; **13**: 499–510.
6. Perez-Shibayama C, Islander U, Lutge M, *et al*. Type I interferon signaling in fibroblastic reticular cells prevents exhaustive activation of antiviral $CD8^+$ T cells. *Sci Immunol* 2020; **5**: eabb7066.
7. Rodda LB, Lu E, Bennett ML, *et al*. Single-cell RNA sequencing of lymph node stromal cells reveals niche-associated heterogeneity. *Immunity* 2018; **48**: 1014–1028.e1016.
8. Camara A, Cordeiro OG, Alloush F, *et al*. Lymph node mesenchymal and endothelial stromal cells cooperate via the RANK-RANKL cytokine Axis to shape the sinusoidal macrophage niche. *Immunity* 2019; **50**: 1467–1481.e1466.
9. Camara A, Lavanant AC, Abe J, *et al*. CD169+ macrophages in lymph node and spleen critically depend on dual RANK and LTbetaR signaling. *Proc Natl Acad Sci USA* 2022; **119**: e2108540119.
10. Mondor I, Baratin M, Lagueyrie M, *et al*. Lymphatic endothelial cells are essential components of the subcapsular sinus macrophage niche. *Immunity* 2019; **50**: 1453–1466.e1454.
11. Pikor NB, Morbe U, Lutge M, *et al*. Remodeling of light and dark zone follicular dendritic cells governs germinal center responses. *Nat Immunol* 2020; **21**: 649–659.
12. Jarjour M, Jorquera A, Mondor I, *et al*. Fate mapping reveals origin and dynamics of lymph node follicular dendritic cells. *J Exp Med* 2014; **211**: 1109–1122.
13. Weber M, Hauschild R, Schwarz J, *et al*. Interstitial dendritic cell guidance by haptotactic chemokine gradients. *Science* 2013; **339**: 328–332.
14. Link A, Vogt TK, Favre S, *et al*. Fibroblastic reticular cells in lymph nodes regulate the homeostasis of naive T cells. *Nat Immunol* 2007; **8**: 1255–1265.
15. Huang HY, Rivas-Caicedo A, Renevey F, *et al*. Identification of a new subset of lymph node stromal cells involved in regulating plasma cell homeostasis. *Proc Natl Acad Sci USA* 2018; **115**: E6826–E6835.
16. Sitnik KM, Wendland K, Weishaupt H, *et al*. Context-dependent development of lymphoid stroma from adult $CD34^+$ adventitial progenitors. *Cell Rep* 2016; **14**: 2375–2388.
17. Alexandre YO, Schienstock D, Lee HJ, *et al*. A diverse fibroblastic stromal cell landscape in the spleen directs tissue homeostasis and immunity. *Sci Immunol* 2022; **7**: eabj0641.
18. Denton AE, Carr EJ, Magiera LP, Watts AJB, Fearon DT. Embryonic FAP+ lymphoid tissue organizer cells generate the reticular network of adult lymph nodes. *J Exp Med* 2019; **216**: 2242–2252.
19. Choi SY, Bae H, Jeong SH, *et al*. YAP/TAZ direct commitment and maturation of lymph node fibroblastic reticular cells. *Nat Commun* 2020; **11**: 519.
20. Chai Q, Onder L, Scandella E, *et al*. Maturation of lymph node fibroblastic reticular cells from myofibroblastic precursors is critical for antiviral immunity. *Immunity* 2013; **38**: 1013–1024.

21. Bogdanova D, Takeuchi A, Ozawa M, *et al*. Essential role of canonical NF-kappaB activity in the development of stromal cell subsets in secondary lymphoid organs. *J Immunol* 2018; **201**: 3580–3586.
22. Pikor NB, Cheng HW, Onder L, Ludewig B. Development and immunological function of lymph node stromal cells. *J Immunol* 2021; **206**: 257–263.
23. Alexandre YO, Mueller SN. Splenic stromal niches in homeostasis and immunity. *Nat Rev Immunol* 2023; **23**: 705–719.
24. Alexandre YO, Devi S, Park SL, Mackay LK, Heath WR, Mueller SN. Systemic inflammation suppresses lymphoid tissue remodeling and B cell immunity during concomitant local infection. *Cell Rep* 2020; **33**: 108567.
25. Cremasco V, Woodruff MC, Onder L, *et al*. B cell homeostasis and follicle confines are governed by fibroblastic reticular cells. *Nat Immunol* 2014; **15**: 973–981.
26. Schumann K, Lammermann T, Bruckner M, *et al*. Immobilized chemokine fields and soluble chemokine gradients cooperatively shape migration patterns of dendritic cells. *Immunity* 2010; **32**: 703–713.
27. Jiang L, Yilmaz M, Uehara M, *et al*. Characterization of leptin receptor^{+} stromal cells in lymph node. *Front Immunol* 2021; **12**: 730438.
28. Astarita JL, Cremasco V, Fu J, *et al*. The CLEC-2-podoplanin axis controls the contractility of fibroblastic reticular cells and lymph node microarchitecture. *Nat Immunol* 2015; **16**: 75–84.
29. Acton SE, Farrugia AJ, Astarita JL, *et al*. Dendritic cells control fibroblastic reticular network tension and lymph node expansion. *Nature* 2014; **514**: 498–502.
30. Horsnell HL, Tetley RJ, De Belly H, *et al*. Lymph node homeostasis and adaptation to immune challenge resolved by fibroblast network mechanics. *Nat Immunol* 2022; **23**: 1169–1182.
31. Assen FP, Abe J, Hons M, *et al*. Multitier mechanics control stromal adaptations in the swelling lymph node. *Nat Immunol* 2022; **23**: 1246–1255.
32. Yang CY, Vogt TK, Favre S, *et al*. Trapping of naive lymphocytes triggers rapid growth and remodeling of the fibroblast network in reactive murine lymph nodes. *Proc Natl Acad Sci USA* 2014; **111**: E109–E118.
33. de Winde CM, Makris S, Millward LJ, *et al*. Fibroblastic reticular cell response to dendritic cells requires coordinated activity of podoplanin, CD44 and CD9. *J Cell Sci* 2021; **134**: jcs258610.
34. Novkovic M, Onder L, Cupovic J, *et al*. Topological small-world Organization of the Fibroblastic Reticular Cell Network Determines Lymph Node Functionality. *PLoS Biol* 2016; **14**: e1002515.
35. Cardani-Boulton A, Sung SJ, Petri WA Jr, Hahn YS, Braciale TJ. Leptin receptor deficiency impairs lymph node development and adaptive immune response. *J Immunol* 2024: ji2100985.
36. De Martin A, Stanossek Y, Lutge M, *et al*. PI16^{+} reticular cells in human palatine tonsils govern T cell activity in distinct subepithelial niches. *Nat Immunol* 2023; **24**: 1138–1148.

SUPPORTING INFORMATION

Additional supporting information may be found online in the Supporting Information section at the end of the article.